ARTICLE

Imaging of the Structure of the Argon and Neon Dimer, Trimer, and Tetramer

B. Ulrich,[†] A. Vredenborg,[†] A. Malakzadeh,[†] L. Ph. H. Schmidt,[†] T. Havermeier,[†] M. Meckel,[†] K. Cole,[†] M. Smolarski,[‡] Z. Chang,[§] T. Jahnke,[†] and R. Dörner*,[†]

[†]Institut für Kernphysik, Goethe Universität, Max-von-Laue-Strasse 1, 60486 Frankfurt, Germany

[‡]Department Physik, ETH Zürich, Wolfgang-Pauli-Strasse 16, 8093 Zürich, Switzerland

[§]Physics Department, Kansas State University, 116 Cardwell Hall, Manhattan, Kansas 66506, United States

ABSTRACT: We Coulomb explode argon and neon dimers, trimers, and tetramers by multiple ionization in an ultrashort 800 nm laser pulse. By measuring all momentum vectors of the singly charged ions in coincidence, we determine the ground state nuclear wave function of the dimer, trimer, and tetramer. Furthermore we retrieve the bond angles of the trimer in position space by applying a classical numerical simulation. For the argon and neon trimer, we find a structure close to the equilateral triangle. The width of the distribution around the equilateral triangle is considerably wider for neon than for argon.
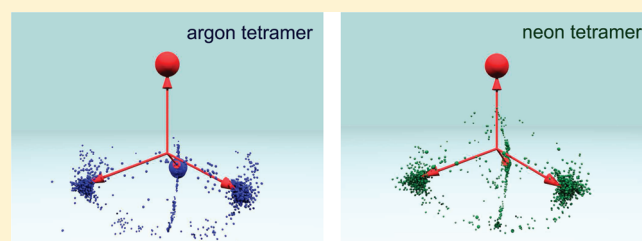
I. INTRODUCTION

The di-, tri-, and tetraatomic rare gas clusters are weakly bound systems that arise from the attractive van der Waals force. The binding energies and potential energy curves of argon and neon dimers have been determined by several theoretical calculations[1−3] in excellent agreement with experimental results using rotational spectroscopy.[4−7] For the argon and neon trimer the ground state configuration is predicted to be an equilateral triangle with an edge length of $R_{Ar_3} = 3.83$ Å and $R_{Ne_3} = 3.32$ Å, respectively.[8] However no experimental spectroscopic studies are available for the trimers.[9]

In this work we employ Coulomb explosion imaging to directly map the ground state wave function of the dimer, trimer, and tetramer. This technique was pioneered in accelerator based experiments by Varger and collaborators[10] who passed high-energy molecular ions through a thin foil to strip off many electrons breaking all bonds. The multiply charged ions then behave like point charges and repel each other. The final momentum vectors of all fragments are then measured in coincidence, and the internuclear distances and bond angles can be retrieved from these data.[11] Instead of stripping by fast traversal through a foil, the electrons can also be stripped off by multiple ionization by synchrotron light,[12−14] by ion impact,[15−17] or by a short intense laser pulse.[18−21] For such laser-based Coulomb explosion imaging which we use in the present study, the laser pulse must be short enough to avoid nuclear motion during the pulse.

II. EXPERIMENT

For our experimental investigation we employed a standard cold target recoil ion momentum spectroscopy (COLTRIMS) setup[22,23] to measure the three-dimensional (3D) momentum vector of all ions in coincidence with a collection solid angle of 4π.

The ionic fragments created in the laser focus were guided by a homogeneous electric field of 8 V/cm toward a position-sensitive detector consisting of two multichannel plates and a multi-hit-capable delay-line anode for position readout. From the time-of-flight (TOF) and the position of impact on the detector, the 3D momentum vector was determined for each particle. As a source for the argon and neon clusters, a supersonic jet was generated by driving the corresponding gas through a 30 μm nozzle at a pressure of several bar. The parameters of the supersonic expansion were chosen such that most of the beam consisted of monomers with a fraction of about 1−2% of dimers and a smaller fraction of trimers and tetramers. For the generation of argon dimers the driving pressure was adjusted to 2 bar whereas for the neon gas we used a higher driving pressure of 8 bar and precooled the nozzle to 163 K. The laser pulses were generated from a multipass amplified Ti: sapphire laser (KM-Laboratories Dragon) with a mean wavelength of 780 nm, at 8 kHz repetition rate, and a temporal pulse width of 35 fs. The linearly polarized laser beam was focused by a parabolic mirror with 7.5 cm focal length into the supersonic gas jet. The laser peak intensity was determined by the ratio of Ar^{2+}/Ar^{+}[24] and the branching ratios of H_2^+ dissociation channels[25] to be 3×10^{14} W cm^{-2} for the argon measurement. For the case of neon, we estimate an intensity of 2.4×10^{15} W cm^{-2} from the Ne^{2+}/Ne^+ ratio.[26] The ion momenta of the fragmentation were calibrated using the kinetic energy release (KER) spectrum from Coulomb exploded N_2 which exhibits a distinct peak structure.[27]
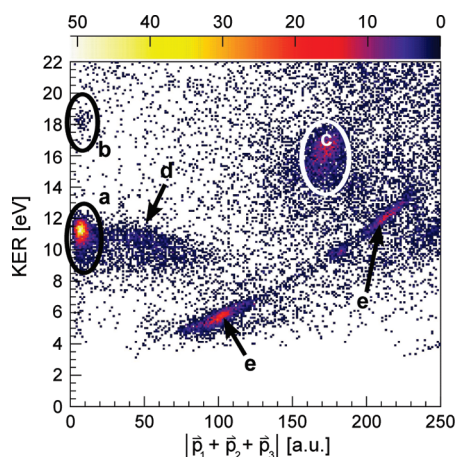
Figure 1. Density plot of the magnitude of the vector momentum sum of the three Ar$^+$ ions (horizontal axis) vs their total KER (vertical axis) for linearly polarized light at an intensity of 3×10^{14} W/cm^2. Coincident Ar$^+$ ions are located close to zero, and thus real coincidences can be distinguished from random ones. The events in region (a) result from instantaneous Coulomb explosion of the trimer following single ionization of each atom. Region (b) comes from events where one of the atoms was originally doubly ionized. Due to a charge-induced dipole interaction, such a trimer exhibits an attractive potential causing the trimer to shrink before—at some smaller internuclear distance—a redistribution of the charges leads to Coulomb explosion. Region (d) is the results for tetramers where one of the atoms remained neutral and cloud (c) is from tetramers where the fourth atom was also charged and therefore carried momentum. The curved structures (e) are coming from false coincidences that could not be unambiguously identified.

III. DATA SORTING

The first step in the data analysis of a many body breakup is to gather all fragments and to clean the data from random events. As most measured ionization events are from monomers, it is important to distinguish Coulomb exploded di-, tri-, and tetramer clusters from random coincidences of two, three, or four monomers ionized in the same laser pulse. In Figure 1 we show a density plot of the magnitude of the ion center-of-mass momentum $p_{cm} = |\vec{p}_1 + \vec{p}_2 + \vec{p}_3|$ of three Ar$^+$ ions versus their total KER. Events with a KER <3 eV are not shown in this spectrum, because we restrict the kinetic energy of each single ion to be >1 eV. Thus we can ensure that the fragment really arises from a Coulomb explosion. This spectrum allows us to distinguish real coincidences from random ones and select only the former for further analysis. If the three ions originate from the same argon trimer, their sum momentum will be close to zero. Thus, real coincidences lie in a stripe near zero sum momentum and can be selected by requiring the center-of-mass momentum of the ions to be $|p_{cm}| < 12$ au With this requirement we also sort out ionization events from isotopically mixed clusters. However, we are unable to completely exclude contamination by Ar$_4$ dissociating into three singly charged and a neutral argon atom with very small momentum given to the neutral. These events appear as a horizontal stripe at 11 eV and are situated in the area marked with a "d". The spectrum also shows the breakup of the argon tetramer into four singly charged ions. This feature is marked with a "c" and lies far away from the zero sum momentum as only three of the four particles are plotted. Figure 1 also contains random coincidences of unclear origin. These are represented by the curved features marked with an "e".
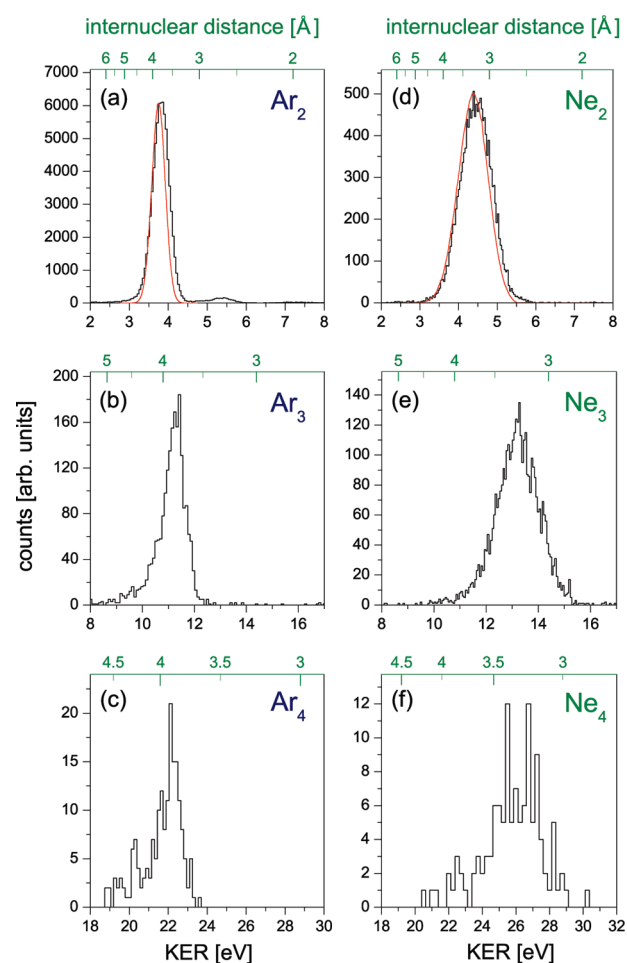

Figure 2. KER distribution for the ions of the argon dimer (a), trimer (b), and tetramer (c) at an intensity of 3×10^{14} W/cm^2 and for the neon dimer (d), trimer (e), and tetramer (f) at an intensity of 2.4×10^{15} W/cm^2. The red solid lines for the argon (a) and neon dimer (d) show the quantum calculation of the KER (eq 2). The upper green axis represents the calculated internuclear distance assuming an equilateral cluster configuration and the classical physics reflection approximation (see text).

For the argon trimer breakup channel the spectrum reveals two features marked "a" and "b". The dominant peak is located around 11.3 eV, while a weaker maximum can be found around 18.5 eV. For all cluster fragmentation channels, we thoroughly select all Coulomb exploded fragments from randoms in this way.

IV. RESULTS AND DISCUSSION

In Figure 2 we show the KER distributions of the argon and neon di-, tri-, and tetramer. For the argon dimer in Figure 2a, we obtain a KER distribution with a peak around 3.82 eV. The ionization process leading to the events in this peak is ultrafast sequential tunneling as discussed in detail in refs 28 and 29. The counts around 5.34 eV arise either from an ionization channel in which one atom of the argon dimer is doubly ionized allowing the dimer to shrink before a redistribution of the charges leads to Coulomb explosion or from a two-side tunnel ionization which is accompanied by an excitation to a potential energy curve that is steeper than $1/R$. For further details see refs 28 and 29.

The KER distribution of the neon dimer in Figure 2d shows a maximum around 4.47 eV and is broader than the distribution of the Ar_2. Again the ionization process is a sequential tunnel ionization. In the approximation of classical physics the internuclear separation at the instant of ionization can be obtained from the KER as $R = 1/KER$ (atomic units are used). These values of R are given in the upper axis labels of Figure 2.

As the pulse length is quite long one might expect the sequential ionization to involve nuclear dynamics as shown in previous studies from Matsuda et al.[21] For the argon dimer this effect is negligible as the mass of the argon atoms is very high.[30] Furthermore the high equilibrium internuclear distance of the atoms for Ar_2 and Ne_2 in combination with the shallow potential energy curves of these van der Waals bound species does not allow for nuclear motion during the short pulse. In a simple model we calculated the trajectory of a classical particle launched from the equilibrium distance on the most attractive Ne_2^+ potential energy curve. For a 35 fs pulse we found an additional KER of 0.5 eV at most. Thus the KER distribution reflects the ground state wave function of the Ar_2 and Ne_2 as the short pulse length almost "freezes" the nuclear motion of the dimer. This classical reflection approximation[13,31] was used in various Coulomb explosion imaging experiments.[10,19] The exact quantum mechanical KER distribution however is determined by calculating the overlap of the bound initial state wave function $\Psi_i(R)$ of the dimer with the continuum wave function $\Psi_f^{KER}(R)$ for a fixed KER. The probability distribution $P(KER)$ is then given by

$$P(KER) = \left| \int dR \, \Psi_i(R) \Psi_f^{KER}(R) \right|^2 \qquad (1)$$

The red solid lines in panels a and d of Figure 2 show the quantum mechanical sampling of the ground state wave function. The slight shift of the experimental data toward higher KER lies below 4.5%. This discrepancy either could arise due to our KER calibration method or could be caused by an enhancement of ionization at lower internuclear distances. We estimate the systematical error for our KER to be equivalent to $KER = \pm 0.11$ eV (3%). Thus the difference between experiment and theoretical calculations is suspected to be caused by the ionization process.

For the determination of the average bond length of the argon dimer, we calculate the internuclear distance for each KER value of Figure 2 and estimate the center-of-mass of this distribution. We receive a value of $R_{Ar_2} = 3.8$ Å which is close to the theoretical prediction of the potential minimum of $R_{Ar_2} = 3.767$ Å.[2] The average internuclear distance of the neon dimer atoms we determine to be about $R_{Ne_2} = 3.3$ Å, which is also in the range of the calculated potential minimum of $R_{Ne_2} = 3.12$ Å.[3]

For the argon trimer the KER distribution in Figure 2b shows a peak around 11.4 eV with a larger width than the KER distribution of Ar_2. In the case of a trimer breakup the determination of the internuclear distance between the three particles from the KER alone requires the knowledge of the geometrical configuration of the argon trimer. However, it is striking that the maximum KER of the trimer is almost equal to $3 \times KER_{Ar_2}$. This finding is in good agreement with different theoretical studies suggesting the predominance of an equilateral trimer structure with an average side length of around $R_{Ar_3} = 3.83$ Å[8] or $R_{Ar_3} = 3.91 \pm 0.20$ Å.[32] Moreover it supports a fast ionization process to be responsible for this breakup. In this case all bonds break simultaneously not leaving the trimer time for nuclear motion. For an equilateral
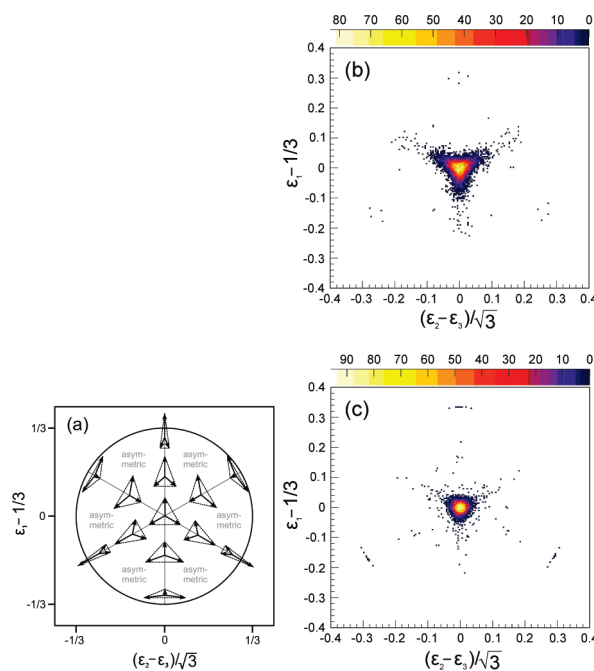

Figure 3. (a) Dalitz plot with geometrical configurations of the momentum vectors for certain regions. In the case of equal mass particles, the Dalitz plot exhibits a 6-fold symmetry. Adapted from ref 34. Dalitz plot for the experimental data for the neon trimer (b) and the argon trimer (c). The entries in the middle of the plot correspond to an equilateral triangular configuration of the momentum vectors at the moment of ionization. The Ne_3 exhibits a broader distribution as a result of a larger variety of triangular configurations in position space.

triangle, classical mechanics gives $R = 3/KER$. This is shown on top of Figure 2b. We determine the average internuclear distance of the trimer in the same way as for the dimer and receive a value of about $R_{Ar_3} = 3.8$ Å. This is just a rough estimate as it does not take into account other possible configurations. For the neon trimer the same signatures as for the argon trimer are observed. First, a broadening of the KER distribution compared to the KER of Ne_2 and second a maximum at about 13.29 eV which is approximately $3 \times KER_{Ne_2}$. Thus the internuclear distance is calculated to be about $R_{Ne_3} = 3.3$ Å (labels on top of Figure.2e) in good agreement with theory $R_{Ne_3} = 3.31$[8] or $R_{Ne_3} = 3.37 \pm 0.34$ Å.[32]

For a further investigation of the geometrical configuration of the trimer, we present our argon and neon trimer data in Figure 3 in a Dalitz plot.[33] This probability-density plot allows visualizing the full kinematics of a three particle breakup by plotting the relative energy ε of each fragment on an equilateral triangle coordinate system. The relative energy of a fragment is defined as its kinetic energy as a fraction of the total breakup energy: $\varepsilon_i = \vec{p}_i^2 / (2m(KER))$ and is displayed as the perpendicular height of the corresponding triangle side. In terms of Cartesian coordinates the vector correlation is mapped by

$$\varepsilon_1 - 1/3 \quad vs \quad (\varepsilon_2 - \varepsilon_3)/\sqrt{3} \qquad (2)$$

Due to momentum conservation the events are restricted to lie within a circle of radius 1/3. Each entry in this plot can be assigned to a geometrical configuration of the momentum vectors. This is shown schematically in Figure 3a for the case of a three-body breakup with equal mass particles.

Comparison of this Dalitz plot with our experimental data from the main decay channel of the argon and neon trimer in Figure 3 reveals mainly an equilateral triangle. It is striking that the neon trimer (upper panel in Figure 3) exhibits a broader distribution which is consistent with the broader KER distribution of the neon trimer in comparison with Ar_3. We attribute this signature to arise from a larger variety of triangular configurations in the position space leading to a broader distribution in momentum space. The neon trimer is floppier compared to the argon trimer, which is expected due to the smaller mass of the atoms and the shallower interaction potentials favoring a broader range of internuclear distances. Beside the dominant equilateral triangular structure of the momentum vectors represented by the area with the highest density in the middle of the Dalitz plot, we observe tails that mainly belong to isosceles triangular configurations.

From this findings we cannot directly draw any conclusion about the geometrical configuration of the trimer in position space, as the Coulomb forces leading to the momenta of the fragments do not transform linearly to position space. Since the distances are large compared to the size of the atomic orbitals, to a good approximation the potential between the three ions can indeed be considered to be purely Coulombic.

We assume the geometry of the argon and neon trimer to be in the ground vibrational state corresponding to an equilateral triangular configuration with an edge length of $R_{Ar_3} = 3.8$ Å and $R_{Ne_3} = 3.3$ Å, respectively.[8] In a classical calculation we determine the forces and momenta of this initial geometry simulating the three-body Coulomb explosion as described in refs 21 and 35. Each component of the calculated momentum vector is then compared on an event-by-event basis with the three measured momentum vectors. To allow for comparison, the measured momentum vectors are adapted to the simulation by rotating them as in a Newton plot (see below). If the difference of measured and calculated value is larger than 0.01 of the absolute value, the triangular side length is iteratively readjusted in position space and the momenta are determined again. This is repeated until a good match for all momentum components of the trimer is found. In contrast to the numerical simulation of ref 21, this procedure includes the variation of all bond lengths of the trimer.

In Figure 4 we show the distribution of the bond angles for the argon and neon trimer in position space retrieved from this method. For comparison a theoretical calculation of Gonzaléz et al.[8] is shown. They studied the trimer states of He, Ne, and Ar by using a variational method in terms of atom pair coordinates and distributed Gaussian basis functions.

For the neon trimer a good accordance with the theory is achieved. Obviously the neon trimer exhibits a broader angular distribution compared to the argon trimer. This was already expected from the Dalitz plot in Figure 3. Gonzaléz et al. calculated the probability of the neon trimer ground state to exhibit an equilateral triangular arrangement to be only 31.6%, whereas other triangular configurations like isosceles (45%) and scalene (23.4%) are also very common. In the case of argon the discrepancy between the experimental data and the theory (red solid line) is evident. For the argon trimer ground state the theory predicts a clear dominance of the equilateral triangular configuration with a probability of 71.1%. Thus, an average angle of 60° and a rather narrow angular distribution is expected. In comparison to our data, however, the maximum of the Ar_3 angular distribution is slightly shifted to smaller angles and exhibits a bigger full width at half-maximum (fwhm).
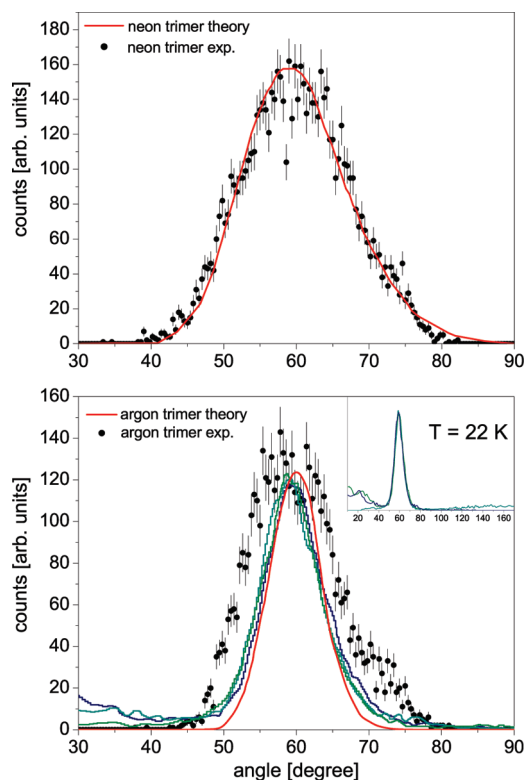

Figure 4. Angular distribution of the Ne_3 (upper panel) and Ar_3 (lower panel) in position space retrieved from the momentum vectors by a numerical model (dots). The red solid lines show the angular distributions of the corresponding trimer ground states $k = 0$ calculated by ref 8. The blue/green/cyan solid lines represent a theoretical calculation of the three angles for the Ar_3 system at a temperature of 22 K from ref 36. The inset shows that the system explores floppier configurations at this temperature.

As a reasonable explanation for this difference, we suspect our gas jet to contain not only argon trimers in the ground state but also excited vibrational states. The first vibrational state of Ar_3 is only 3.9 meV above the ground state. On the basis of the translational beam offset of the argon monomer compared to residual gas particles, we can estimate the internal jet temperature to be $T \approx 7$ K. At this temperature the argon momentum distribution in the jet direction is 3 au (fwhm), corresponding to about 2 meV of energy transfer in a binary collision. This makes it likely that our trimers are not all in the ground vibrational state. Considering the calculated triangular arrangements of the first excited Ar_3 state with an reduced probability of 52.5% for an equilateral structure and a higher appearance of isosceles (32.9%) and scalene (14.6%) triangles would cause a broadening of the distribution.[8] The same would apply for the neon trimer, whose internal jet temperature is determined to be also 7 K. For the neon trimer the first vibrational state is only 2.0 meV above the ground state, but unlike the argon trimer the triangular configuration of the Ne_3 vibrational state does not change much.

A recent path-integral Monte Carlo study on Ar_3 for temperatures between 0 and 40 K found a temperature dependency in the configuration of argon trimers.[36] For temperatures beyond $T \sim 20$ K they found the argon trimer to exhibit floppier configurations than the rigid equilateral geometry. For comparison, we show the calculated angular distribution of Ar_3 at 22 K in Figure 4 as blue/green/cyan solid lines. The inset of Figure 4
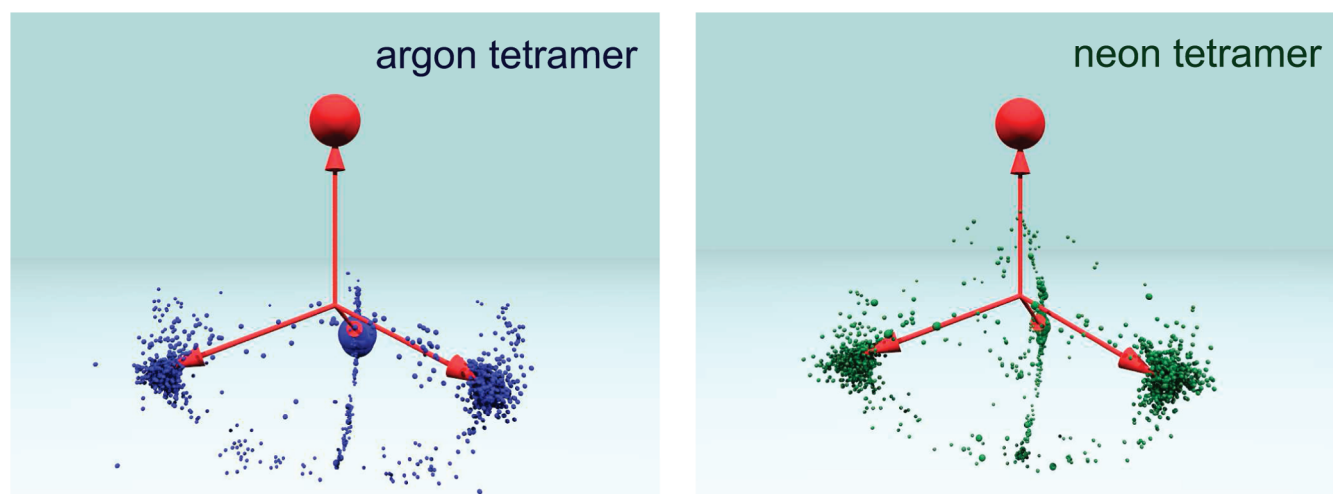
6939

dx.doi.org/10.1021/jp1121245 |*J. Phys. Chem. A* 2011, 115, 6936–6941

Figure 5. Newton diagram for the four particle breakup of Ar_4 (left panel) and Ne_4 (right panel). The momentum of the first ion in the center of mass frame is represented by the red sphere. The relative momentum vectors of the second, third, and fourth ions are mapped underneath. By definition all entries corresponding to the momentum vector on the far side are forced to lie on a vertical plane. The radii of all spheres are proportional to the density of entries.

shows that even linear configurations are found at this temperature. Even though the main peak is slightly shifted and broaden, it does not reproduce our data. This confirms the estimation of our jet temperature to be below 22 K. The potential reason for the remaining difference between our position space data and the calculations is experimental resolution or potentially the classical approximation used to convert from momentum to position space.

In panels c and f of Figure 2, we present the KER distribution for the argon and neon tetramer, respectively. This breakup channel is very weak due to the smaller fraction of tetramer clusters in the supersonic gas jet and the lower coincidence efficiency for a four particle breakup. For this four-body break-up channel we require the center-of-mass momentum of the ions to be $p_{cm} = |\vec{p}_1 + \vec{p}_2 + \vec{p}_3 + \vec{p}_4| < 12$ au For the Ar_4 we obtain a KER distribution with a maximum around 22.4 eV, which corresponds approximately to $6 \times KER_{Ar_2}$. This is in line with the assumption of a cluster configuration with six equilateral internuclear distances, as it is provided by a triangular pyramid. On top of panels c and f of Figure 2 the internuclear distances of such an atomic arrangement are calculated leading to an average value of 3.85 Å. The same applies to the neon tetramer whose KER peak around 26.7 eV corresponds to a side length of 3.2 Å.

To visualize the real configuration of the tetramer in momentum space, we generalize the Newton plot to three dimensions (see Figure 5). Here all momenta are shown with respect to the center of mass frame and are normalized to the first fragment, which is now fixed at the origin of the coordinate system pointing upward in the direction of the red sphere. The remaining three fragments are defined within the plotting area underneath. The so defined Newton plot is shown in Figure 5 for the argon tetramer (left panel) and the neon tetramer (right panel) in a three-dimensional diagram. By definition all entries corresponding to the momentum vector on the far side are forced to lie on a vertical plane. The radii of all spheres are chosen to be proportional to the number of entries. Comparison of the argon and neon tetramer shows that the distribution of the momentum vectors of the neon tetramer is slightly broader than that for argon. If we connect the areas with the highest density, we receive a triangular pyramid. All events that lie far away from the highest density spots are attributed to an ionization process in which the atoms of the tetramer do not

break simultaneously but involve a very short time of dissociation. These events are characterized by a slightly lower KER than the entries close to the edge of the triangular pyramid.

V. CONCLUSION

In conclusion we have used laser Coulomb explosion imaging to study the structure of small Ne and Ar cluster. Our data confirm the predicted bond length of the dimer within the precision of our experiment. For the trimer we find a mainly equilateral triangular distribution. The angular distribution of the neon trimer is in excellent agreement with the theoretical calculations. However for the argon trimer we observe a broader angular distribution than that predicted by theory. We attribute this to be caused either by the experimental resolution or by the limit of the classical calculation of the bond angles. The neon trimer is found to be significantly floppier than that of argon, with the width of the bond angle distribution broader than for argon. The tetramer is shown to have a triangular pyramid structure.

The superb background suppression of our multiparticle detection technique will allow us to perform a similar study on small helium clusters in the future. For the helium trimer already for the ground state the geometry is disputed.[8,37−39] Even more a point of controversial discussion is the existence of a first excited state of the trimer which has Efimov character. This Efimov trimer has escaped experimental observation until today.[40] The technique used in the present study is an extremely powerful tool to search for this elusive Efimov state of the helium trimer. Such experiments are currently under way in our laboratory.

■ AUTHOR INFORMATION

Corresponding Author
*E-mail: Doerner@atom.uni-frankfurt.de.

6940

dx.doi.org/10.1021/jp1121245 |*J. Phys. Chem. A* 2011, 115, 6936–6941

■ REFERENCES

(1) Tao, F. M.; Pan, Y. K. *Mol. Phys.* **1994**, *81*, 507.

(2) Patkowski, K.; Murdachaew, G.; Fou, C.; Szalewicz, K. *Mol. Phys.* **2005**, *103*, 2031–2045.

(3) Tao, F. M.; Pan, Y. K. *Chem. Phys. Lett.* **1992**, *194*, 162.

(4) Herman, P. R.; LaRocque, P. E.; Stoicheff, B. P. *J. Chem. Phys.* **1988**, *89*, 4535.

(5) Tanaka, Y.; Yoshino, K. *J. Chem. Phys.* **1970**, *53*, 2012.

(6) Tanaka, Y.; Yoshino, K. *J. Chem. Phys.* **1972**, *57*, 2964.

(7) Wüest, A.; Merk, I. *J. Chem. Phys.* **2003**, *118*, 8807.

(8) González-Lezana, T.; Rubayo-Soneira, J.; Miret-Artés, S.; Gianturco, F. A.; Delgado-Barrio, G.; Villarreal, P. *J. Chem. Phys.* **1999**, *110*, 9000.

(9) Karlický, F.; Lepetit, B.; Kalus, R.; Gadéa, F. x. *J. Chem. Phys.* **2007**, *126*, 4305.

(10) Vager, Z.; Naaman, R.; Kanter, E. P. *Science* **1989**, *244*, 426.

(11) Kwon, K.; Moscowitz, A. *Phys. Rev. Lett.* **1996**, *77*, 1238.

(12) Muramatsu, Y.; Ueda, K.; Saito, N.; Chiba, H.; Lavolée, M.; Czasch, A.; Weber, T.; Jagutzki, O.; Schmidt-Böcking, H.; Moshammer, R.; Becker, U.; Kubozuka ans, K.; Koyano, I. *Phys. Rev. Lett.* **2002**, *88*, 133002.

(13) Weber, Th.; Czasch, A.; Jagutzki, O.; Müller, A. K.; Mergel, V.; Kheiferts, A.; Rotenberg, E.; Meigs, G.; Prior, M. H.; Daveau, S.; Landers, A.; Cocke, C. L.; Osipov, T.; Díez Muiño, R.; Schmidt-Böcking, H.; Dörner, R. *Nature* **2004**, *431*, 437.

(14) De Fanis, A.; Saito, N.; Machida, M.; Okada, K.; Chiba, H.; Cassimi, A.; Dörner, R.; Koyano, I.; Ueda, K. *Phys. Rev. A* **2004**, *69*, 022506.

(15) Neumann, N.; Hant, D.; Schmidt, L. Ph. H.; Titze, J.; Jahnke, T.; Czasch, A.; Schöffler, M. S.; Kreidi, K.; Jagutzki, O.; Schmidt-Böcking, H.; Dörner, R. *Phys. Rev. Lett.* **2010**, *104*, 103201.

(16) Rajgara, F. A.; Krishnamurthy, M.; Mathur, D.; Nishide, T.; Shiromaru, H.; Kobayashi, N. *J. Phys. B* **2004**, *37*, 1699.

(17) Pešić, Z. D.; Chesnel, J.-Y.; Hellhammer, R.; Sulik, B.; Stolterfoht, N. *J. Phys. B* **2004**, *37*, 1405.

(18) Alnaser, A. S.; Ulrich, B.; Tong, X. M.; Litvinyuk, I. V.; Maharjan, C. M.; Ranitovic, P.; Osipov, T.; Ali, R.; Ghimire, S.; Chang, Z; Lin, C. D.; Cocke, C. L. *Phys. Rev. A* **2005**, *72*, 030702.

(19) Ergler, Th.; Rudenko, A; Feuerstein, B.; Zrost, K.; Schröter, C. D.; Moshammer, R.; Ullrich, J. *Phys. Rev. Lett.* **2005**, *95*, 093001.

(20) Légaré, F.; Lee, K. F.; Litvinyuk, I. V.; Dooley, P. W.; Wesolowski, S. S.; Bunker, P. R.; Dombi, P.; Krausz, F.; Bandrauk, A. D.; Villeneuve, D. M.; Corkum, P. B. *Phys. Rev. A* **2005**, *71*, 013415.

(21) Matsuda, A.; Takahashi, E. J.; Hishikawa, A. *J. Chem. Phys.* **2007**, *127*, 114318.

(22) Ullrich, J.; Moshammer, R.; Dörner, R.; Jagutzki, O; Mergel, V; Schmidt-Böcking, H.; Spielberger, L *J. Phys. B* **1997**, *30*, 2917.

(23) Dörner, R.; Mergel, V.; Jagutzki, O.; Spielberger, L.; Ullrich, J.; Moshammer, R.; Schmidt-Böcking, H. *Phys. Rep.* **2000**, *330*, 95–192.

(24) Weber, Th.; Weckenbrock, M.; Staudte, A.; Spielberger, L.; Jagutzki, O.; Mergel, V.; Afaneh, F.; Urbasch, G.; Vollmer, M.; Giessen, H.; Dörner, R. *J. Phys. A* **2000**, *33*, L 127–L133.

(25) Alnaser, A. S.; Tong, X. M.; Osipov, T.; Voss, S.; Maharjan, C. M.; Shan, B.; Chang, Z.; Cocke, C. L. *Phys. Rev. A* **2004**, *70*, 023413.

(26) Larochelle, S.; Talebpour, a.; Chin, S. L. *J. Phys. B* **1998**, *31*, 1201.

(27) Lundqvist, M.; Edvardsson, D.; Baltzer, P.; Wannberg, B. *J. Phys. B* **1996**, *29*, 1489.

(28) Manschwetus, B.; Rottke, H.; Steinmeyer, G.; Foucar, L.; Czasch, A.; Schmitt-Böcking, H.; Sander, W. *Phys. Rev. A* **2010**, *82*, 013413.

(29) Ulrich, B.; Vredenborg, A.; Malakzadeh, A.; Meckel, M.; Cole, K.; Smolarski, M.; Chang, Z.; Jahnke, T.; Dörner, R. *Phys. Rev. A* **2010**, *82*, 013412.

(30) Stapelfeldt, H.; Sakai, H.; Constant, E.; Corkum, P. B. *Phys. Rev. A* **1997**, *55*, R3319.

(31) Gislason, E. A. *J. Chem. Phys.* **1973**, *58*, 3702.

(32) Rick, S. W.; Lynch, D. L.; Doll, J. D. *J. Chem. Phys.* **1991**, *95*, 3506.

(33) Dalitz, R. H. *Philos. Mag.* **1953**, *44*, 1068.

(34) Galster, U.; Baumgartner, F.; Müller, U.; Helm, H.; Jugen, M. *Phys. Rev. A* **2005**, *72*, 062506.

(35) Kwon, K.; Moscowitz, A. *Phys. Rev. Lett.* **1996**, *77*, 1238.

(36) Pérez de Tudela, R.; Márquez-Mijares, M.; González-Lezana, T.; Roncero, O.; Miret-Artés, S.; Delgado-Barrio, G.; Villarreal, P. *J. Chem. Phys.* **2010**, *132*, 244303.

(37) Lewerenz, M. *J. Chem. Phys.* **1997**, *106*, 4596.

(38) Raman, M. V.; Krishna; Whaley, K. B. *J. Chem. Phys.* **1990**, *93*, 6738.

(39) Rick, S. W.; Lynch, D. L.; Doll, J. D. *J. Chem. Phys.* **1991**, *95*, 3506.

(40) Brühl, R.; Kalinin, A.; Kornilov, O.; Toennies, J. P.; Hegerfeldt, G. C.; Stoll, M. *Phys. Rev. Lett.* **2005**, *95*, 063002.

6941

dx.doi.org/10.1021/jp1121245 |*J. Phys. Chem. A* 2011, 115, 6936–6941